Microstructure and mechanical properties of as-built and heat-treated electron beam melted Ti–6Al–4V

Syed, A., Awd, M., Walther, F. & Zhang, X.

Original citation & hyperlink:
Syed, A, Awd, M, Walther, F & Zhang, X 2019, 'Microstructure and mechanical properties of as-built and heat-treated electron beam melted Ti–6Al–4V' Materials Science and Technology, vol. 35, no. 6, pp. 653-660.
https://dx.doi.org/10.1080/02670836.2019.1580434

DOI 10.1080/02670836.2019.1580434
ISSN 0267-0836
ESSN 1743-2847

Publisher: Taylor and Francis

This is an Accepted Manuscript of an article published by Taylor & Francis in Materials Science and Technology on 19/02/2019, available online: http://www.tandfonline.com/10.1080/02670836.2019.1580434

Material Science and Technology, Accepted on 05 Feb 209, Published online: 19 Feb 2019

https://doi.org/10.1080/02670836.2019.1580434

Microstructure and mechanical properties of as built and heat treated electron beam melted Ti-6Al-4V

Abdul Khadar Syed[*1], Mustafa Awd[2], Frank Walther[2], Xiang Zhang[1]

[1]Faculty of Engineering, Environment and Computing, Coventry University, Coventry CV1 5FB, UK

[2]Department of Materials Test Engineering, TU Dortmund University, 44227 Dortmund, Germany

Email: [*]Abdul.Syed@coventry.ac.uk, mustafa.awd@tu-dortmund.de, frank.walther@tu-dortmund.de, Xiang.Zhang@coventry.ac.uk

Abstract

This paper investigates the effect of post-deposition heat treatment on porosity, microstructure, and mechanical properties of Ti6Al4V produced via an Electron Beam Melting process. Samples were studied in the conditions of as built and heat treated at 920°C and 1030°C. The as built samples are characterised by columnar β grains aligned along the build direction. Within in the columnar β grains, α+β microstructure with Widmanstätten and colony morphologies was found. Heat treatment has resulted in an increase in the α lath width. Tensile tests showed greater yield and ultimate tensile strengths in the as built condition compared to the wrought material. Porosity re-growth was found after heat treatment, but it did not affect the tensile properties. The increase in ductility after heat treatment is mainly associated with the increase in the α lath width that increases the effective slip length.

Keywords: Additive Manufacturing, Electron beam melting, Heat treatment, Microstructure, Tensile properties, Titanium alloys

1 Introduction

Electron Beam Melting (EBM) is a powder bed fusion additive manufacturing process that enables near net shape part production by depositing successive layers of material through melting metal powders using a high-energy electron beam. Amongst various materials deposited by EBM, particular attention has been paid on titanium alloy Ti6Al4V due to its high strength to weight ratio, excellent corrosion resistance and biocompatibility [1]. Material during the EBM process experiences a typical thermal cycle of preheating,

https://doi.org/10.1080/02670836.2019.1580434

melting, and solidification. EBM Ti6Al4V consist of Widmanstätten α+β within epitaxillay grown columnar parent β grains that are aligned parallel to the build direction [2–8]. However, parts build with less than 1 mm wall thickness has a mixed microstructure of α+β and α′ martensite plates [9]. Furthermore, previous studies have also reported a graded microstructure and mechanical properties along the build direction due to variation in the cooling rate from the bottom to the top of the build [10–12].

Mechanical properties of EBM Ti6Al4V is influenced by the process parameters and post-deposition heat treatments. Research reported in [13] found that the tensile and yield strength of as built sample was 5% higher than wrought Ti6Al4V, but the ductility of the former is four times lower than that of the latter. In contrast, Koike *et al.* [14] found the yield strength and tensile strength of as built samples reduced by 15% and 16% respectively compared to wrought. Zhai et *al.* [15] found that the tensile strength and yield strength was 7% and 4% higher and the elongation was 42% lower than wrought. Overall, the yield strength varied from 783 MPa up to 1130 MPa and ductility ranged from 2.3% to 20%. The large variation in mechanical properties of EBM Ti6Al4V is mainly associated with the differences in process parameters that control the porosity and microstructure [8,11].

Another parameter that controls the microstructure hence mechanical properties is the post-deposition heat treatment. However, only very limited research is found on the influence of post-deposition heat treatment on the microstructure and mechanical properties of EBM Ti6Al4V [4,10,16,17]. Amongst these, extra-low interstitial (ELI) Ti6Al4V was studied in [10, 16] that contained reduced levels of oxygen, nitrogen, carbon and iron to increase the ductility of the material and the influence of hot isostatic pressing (HIPing) on tensile and fatigue properties was reported in [17]. Only one study [4] investigated the effect of post-deposition heat treatment on the microstructure and mechanical properties of Ti6Al4V samples built via EBM. Furthermore, no literature is available on the post-deposition heat treatment at above the β transus temperature on the porosity and its consequence on the tensile properties. Therefore, considerable research is still needed to understand the large scatter in the mechanical properties of EBM Ti6Al4V which is a direct consequence of the process induced porosity and microstructure. Hence, this paper aims to investigate the influence of post-deposition heat

https://doi.org/10.1080/02670836.2019.1580434

treatment on the microstructure, porosity and mechanical properties of EBM Ti6Al4V and to develop a relation between the post-deposition heat treatment process, porosity, microstructure and resultant mechanical properties.

2 Materials and methods

The test samples were produced using an ARCAM A2 EBM machine with ARCAM standard process parameters for Ti6Al4V. Gas atomised Ti6Al4V (Grade 5) powder with particle size ranging between 45-100 µm was used to produce the samples. The chemical composition of the powder was (wt %): C=0.015, O=0.18, N=0.026, H=0.003, Fe=0.17, Al=6.12, V=4.04, and balance Ti. The target pre-heat temperature was maintained 700°C throughout the build process. Three flat rectangular plates of length 145 × 45 × 5 mm were deposited with a layer thickness of 50 µm, Fig. 1a. One plate was used to extract the as built samples, one plate for heat treatment at 920°C for 2 hrs followed by air cooling and the final plate for heat treatment at 1030°C for 2 hrs followed by air cooling to room temperature. Heat treatment was carried out in a vacuum controlled environment with a heating rate of 10°C/minute. After heat treatment, three tensile test samples (120 × 10 × 3) were extracted (Fig. 1b) from each plate following the ASTM E8 standard. Prior to extracting the tensile samples, the 5 mm thick plate was reduced to 3 mm to remove the surface defects.

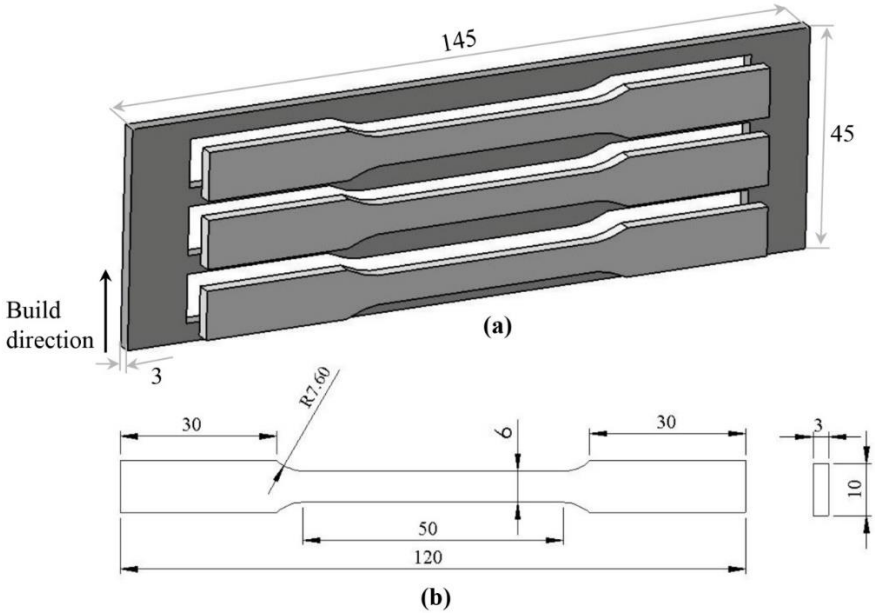

https://doi.org/10.1080/02670836.2019.1580434

Fig 1: Schematic of (a) geometry and tensile test sample extraction (b) dimensions of flat tensile test specimen (unit: mm).

Porosity analysis was carried using X-ray micro-computed tomography (X-ray CT) on small rectangular samples (10 × 6 × 3 mm thick) extracted from each condition. Specimens were subjected to a beam voltage of 132 kV and a current of 51 μA. The effective pixel size was 10 μm that enable to detect defects greater than 20 μm per spatial dimension. Four frames for each projection (2fps) were recorded where each had an exposure time of 500 ms.

For microstructural analysis, the samples were prepared and etched with Kroll's reagent for 45 seconds. The micro texture of the samples was examined by electron backscatter diffraction (EBSD) along the build direction in a measurement area of 1000 × 500 μm^2 and with a step size of 0.1μm. Samples prepared for microstructural analysis were also subjected to Vickers microhardness measurement under 0.5 kgf load for 10 seconds, on both the as built and heat treated samples. For each sample, 30 hardness measurement was made, and the average hardness value is reported.

Tensile tests were conducted using a servo electric machine of capacity 50 kN at a constant displacement rate of 2 mm/min. Sample deformation was measured using a clip-on extensometer of gauge length 25 mm.

3 Results and discussion

3.1 Porosity analysis

Three types of pores were observed; spherical gas pores (Fig. 2a), gas pores filled with partially melted powder particles (Fig. 2b) and irregularly shaped lack of fusion pores (Fig. 2c). Gas pores are formed due to the presence of defects in raw material (hollow powder particles) with entrapped argon gas. Furthermore, vaporisation of low melting point constituents within the alloy also lead to gas pores in the EBM builds [18]. The observed gas pores in as built condition have a mean diameter of 35±12μm. Gas pores filled with partially melt powder were formed due to turbulence in the melt pool and low viscosity liquid metal spattering that ejects away from the melt pool and falls into the molten metal or on the powder bed as stated by [19]. The mean diameter of gas pores filled with partially melted powder particles is 10±3 μm. The lack of fusion pores is the consequence of the partially melted layer that was formed due to insufficient energy density during the deposition in that area. Although material fabrication was carried out

https://doi.org/10.1080/02670836.2019.1580434

using optimised process parameters, external factors such as electromagnetic interference during manufacturing might result in insufficient energy density.

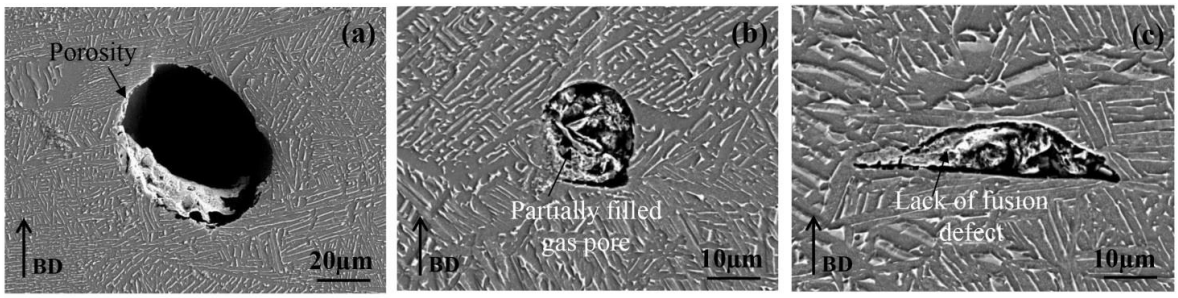

Fig. 2: Secondary electron SEM images of (a) gas pore (b) gas pore filled with partially melted Ti6Al4V (c) a lack of fusion defect filled with partially melted Ti6Al4V.

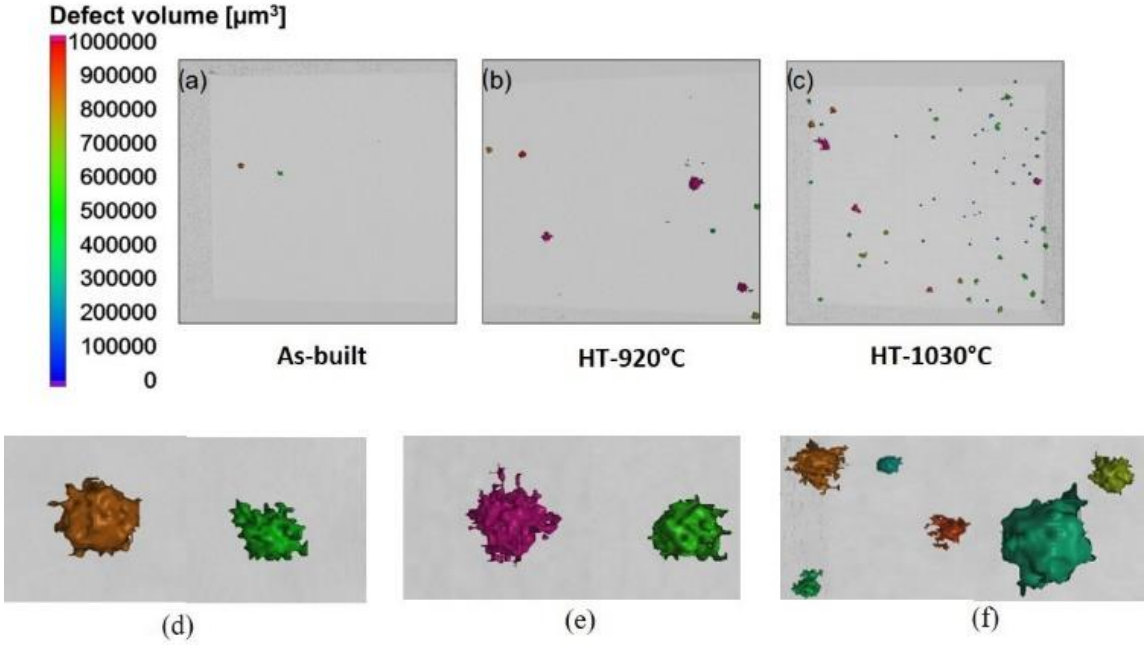

Fig. 3: Volumetric defect distributions of (a) as built (b) HT- 920°C (c) HT-1030°C samples. (d)-(f) high resolution images of as built, HT-920°C and HT-1030°C respectively.

Porosity analysis by X-ray CT is shown in Fig. 3. Most of the pores appear to be spherical in shape (Fig. 3 e-f). The X-ray CT analysis did not show any lack of fusion defects as appeared in 2D micrograph analysis (Fig. 2c). This might be due to the measured size of the lack of fusion defects observed in 2D micrograph analysis is close to the threshold limit (20 µm) of the X-ray CT. The relative density measured on HT-920°C and HT-1030°C samples showed 99.99% and 99.98% respectively. The decrease in density after

https://doi.org/10.1080/02670836.2019.1580434

heat treatment is mainly due to porosity regrowth after the heat treatment. It is evident from Fig. 3 that the pores that are regrown appear to be as gas pores. The argon gas within the gas pores cannot diffuse out from the material and remains in the samples. Upon heat treatment, the internal gas pressure will provide a driving force to regrowth, hence a lower density is observed after heat treatment. Similar results were found in [20]. Post-deposition heat treatment HIPing is very effective to reduce the porosity in EBM build parts [10]. However, HIPping leads to porosity regrowth as observed in [20].

3.2 Microstructure and texture characterisation

3.2.1 As built microstructure

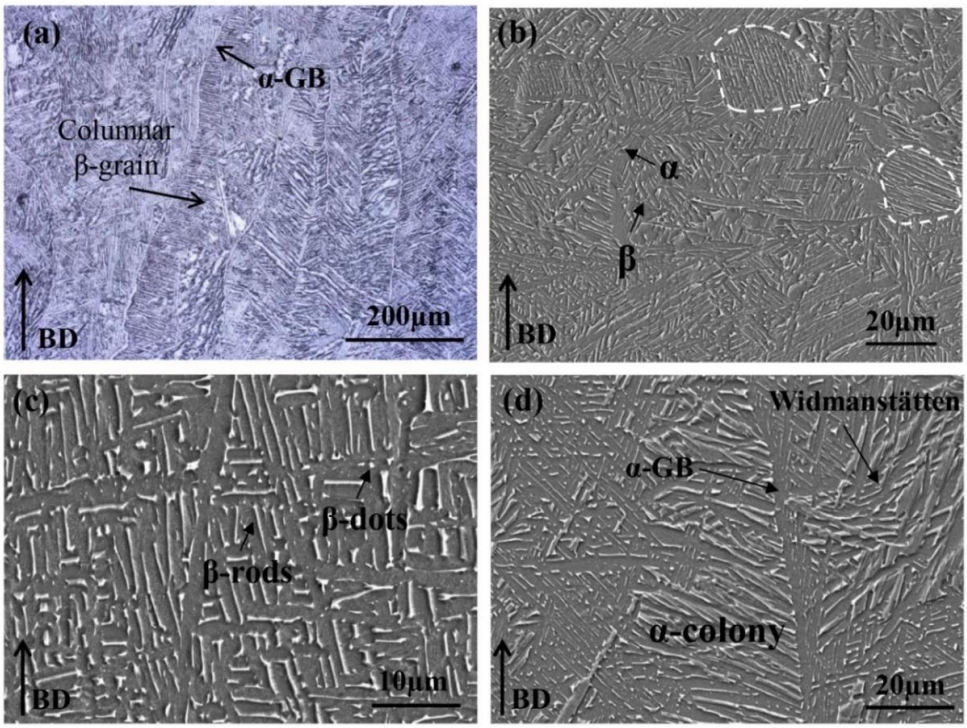

Fig. 4: As built microstructure showing (a) optical micrograph of columnar β grains. SEM image showing (b) α+β microstructure (c) retained β phase formed as discrete flat rods and dots morphology (d) Widmanstätten and colony morphology formed along one α-GB (dark and bright areas show α and β phase respectively).

The bulk microstructure of as built samples are characterised by columnar β grains oriented along the build direction which is a direct consequence of large thermal gradients along the build direction, as shown in Fig. 4a. Columnar β grains consist of α+β microstructure with both Widmanstätten and colony morphology (Fig. 4b). The retained

Material Science and Technology, Accepted on 05 Feb 209, Published online: 19 Feb 2019

https://doi.org/10.1080/02670836.2019.1580434

β appears as rod and dot-like morphology embedded within the α (Fig. 4c). A relatively slow cooling rate from above β leads to a colony of α clusters belonging to the same crystallographic variants whereas faster cooling rates result in Widmanstätten α belong to multiple variants. At intermediate cooling rates, a mixed microstructure is observed [21]. Most α laths are individual and oriented in various directions. Fig. 4d shows two adjacent β grain exhibited two different microstructures, one being Widmanstätten and the second shows a colony morphology. The α grain boundary that observes the Burgers orientation with the β grain develops α colony whereas the grain which did not follow the Burgers orientation relationship develop a Widmanstätten microstructure as reported in [21]. To further characterise the as built microstructure, α lath width measurements were performed by measuring the spacing between two neighbouring β laths (the bright phase showed in Fig. 4c) using the Image J software. The average (100 measurements) α lath width in as built samples was found to be 0.75±0.38 µm.

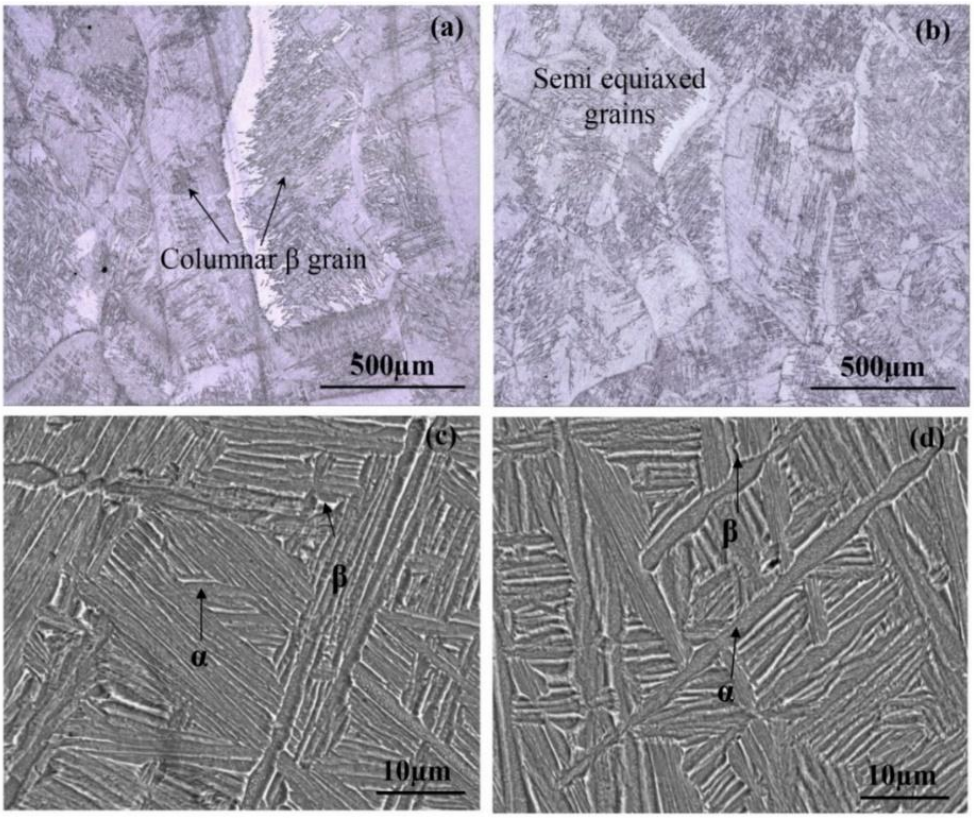

Fig. 5: Optical micrographs of samples heat treated at (a) 920°C showing the columnar grain morphology (b) 1030°C showing semi equiaxed beta grains. SEM images showing microstructure of samples heat treated at (c) 920°C (d) 1030°C.

Material Science and Technology, Accepted on 05 Feb 209, Published online: 19 Feb 2019

https://doi.org/10.1080/02670836.2019.1580434

After heat treatment at 920°C, the columnar morphology of β grain is maintained (Fig. 5a). However, the α lath width increased to 0.94±0.11 μm. Increase in α lath width after post-deposition heat treatment at below β transus temperature was also observed in [16]. Furthermore, α colonies were present after heat treatment (Fig. 5c). Heat treatment at 1030°C followed by air-cooling resulted in α to nucleate at the grain boundaries and then grows as lamellar into the β grain. Depending on the cooling rate, the lamellae are either coarse (slower cooling rate) or fine (faster cooling rate). After heat treatment to 1030°C, α lath width increased to 1.38±0.26 μm. Furthermore, smaller α colonies were observed compared to as built and heat treatment at 920°C conditions.

3.2.2 Texture characterisation

Fig.6 shows texture analysis of as built and heat treated samples. As built sample shows strong crystallographic texture, Fig. 6a. Following the Burgers relation and because of symmetry, 12 possible variant orientations that can form α from a single parent β grain, according to [1,22]. As reported by [4,16] the parent β phase in the as built condition is characterised by the presence of a strong texture in the <100> direction in the build direction. The subsequent deposition of layers will rapidly increase the temperature causing rapid solidification of the β phase at the rear of the moving melt pool. This process is repeated and causing the parent β to grow along the multiple layers. A detailed analysis of the typical texture in EBM Ti6Al4V was investigated by Formanoir et.al.[16] and reported that the β phase typically exhibits cube or rotated cube texture in which one <100> β axis remains aligned with the build direction, whereas the two other <100> β axes are rotated by a specific angle with respect to the macroscopic directions.

https://doi.org/10.1080/02670836.2019.1580434

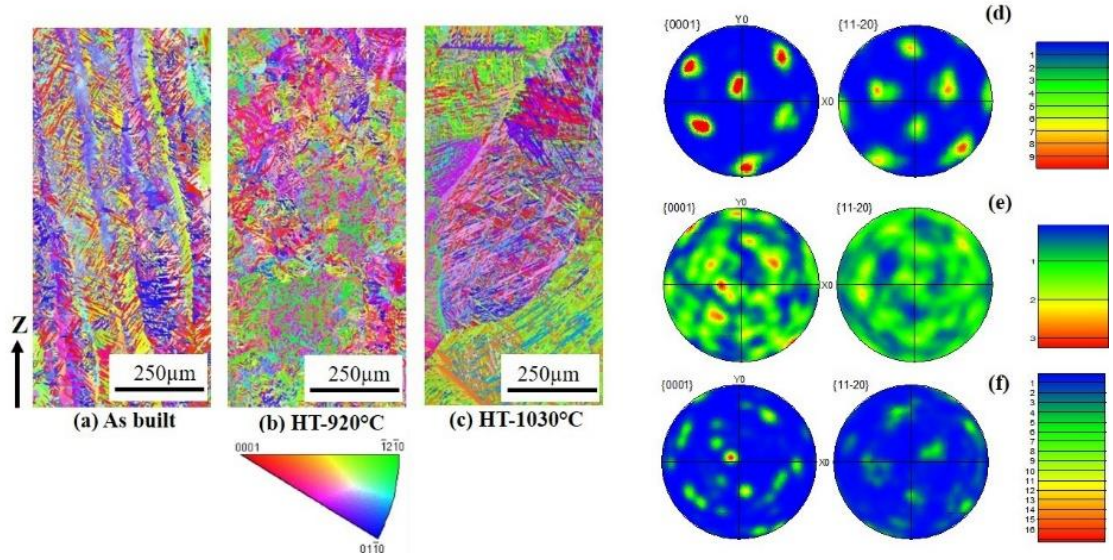

Fig. 6: Texture analysis of as built and heat treated samples

Although the parent β morphology is essentially not modified by HT-920°C, the coarser lamellar due to long exposure to below β transus temperature resulted in a weaker texture, Fig 6b and 6e. On the other hand, HT-1030°C induced a noticeable change in β embedded with large α clusters because of faster cooling. The presence of large α clusters oriented in the same crystallographic direction significantly increased the α texture. According to the Burgers crystallographic relationship, three α variants can be generated from each of the four $<111>_{\beta}$ directions. These α variants sharing the same $[111]_{\beta}$ directions have a tendency to form clusters during a fast cooling rate that can be observed in Fig. 6c and 6f and result in significant texture. However, slower cooling rate (furnace cooling) from above β transus temperature will result in no clustering of the α phase and a weaker texture can be obtained.

3.3 Mechanical properties

As built samples have a higher hardness (380±12 HV), compared to the wrought material (348±7 HV) and heat treated samples due to the fine Widmanstätten microstructure. After heat treatment, a decrease in hardness was found due to the increase in α lath width. i.e. 351±8 and 334±9 HV for HT-920°C and HT-1030°C respectively. It is worth noting the there is a good correlation between the change in microstructure and hardness.

Material Science and Technology, Accepted on 05 Feb 209, Published online: 19 Feb 2019

https://doi.org/10.1080/02670836.2019.1580434

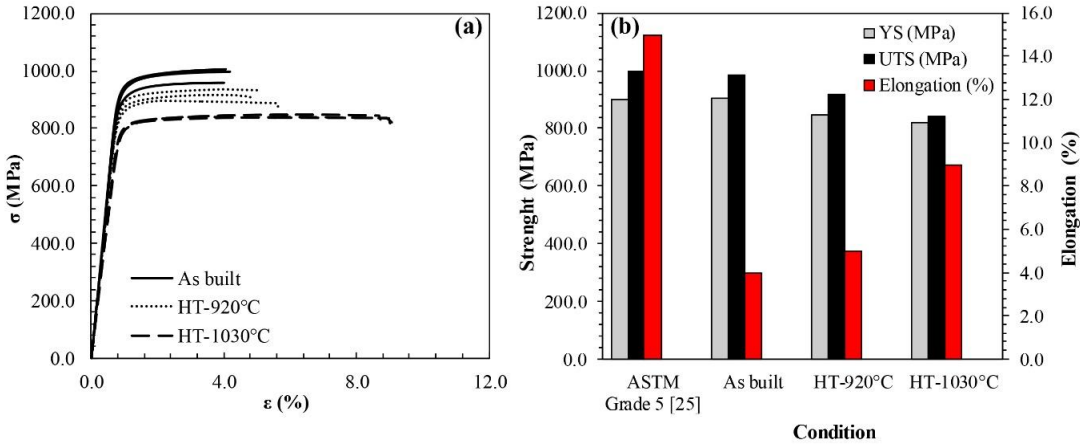

Fig. 7: Tensile properties showing (a) Tensile test stress-strain curves (three test each) (b) comparison of the ultimate tensile strength, yield strength and elongation.

Measured stress-strain curves and tensile properties for as built and heat treated samples compared to the wrought material is presented in Fig. 7. The yield strength and ultimate tensile strengths are 5% and 14% higher and the ductility is 250% lower for as built samples compared to wrought material because of the fine Widmanstätten microstructure thus resulting in much lower plastic deformation before fracture. The ductility of EBM built material is dependent on the build orientation relative to the loading axis [15,17]. In the current work, the build direction (also the β columnar growth direction) was perpendicular to the loading axis and therefore the deformation became highly localised and inhibited due to dislocation pileups at the grain boundaries. In addition, the existence of α laths restricted the dislocation motion along the laths and dislocations may not travel a long enough distance resulting in reduced ductility [23].

After heat treatment at 920°C, the yield strength and ultimate tensile strength reduced by 4% and 7% compared to as built condition. In Ti6Al4V, yield strength and plastic deformation are influenced by the α lath width which determines the slip band length and hence controls the plastic deformation. An increased α lath width was observed after heat treatment at 920°C that has resulted in decreased yield strength and ultimate tensile strength due to the increased effective slip length during the deformation. However, the elongation at failure increased by 25% compared to that of the as built condition though it was still significantly below that of wrought material.

Heat treatment at 1030°C resulted in further reduction of the yield strength and tensile strength by 6% and 9% respectively compared with heat treatment at 920°C and

https://doi.org/10.1080/02670836.2019.1580434

10% and 17% compared to the as built condition. The coarser microstructure will increase ductility, hence the reduction in yield strength and tensile strength owing to the increase in the effective slip length. Nevertheless, ductility increased by 125% and 80% compared with as built and heat treatment at 920°C samples respectively. Overall, the tensile properties of the as built and heat treated EBM Ti6Al4V found in this research are mainly governed by the α lath width that determines the effective slip length. Although porosity regrowth was observed after heat treatment, it appears that the α lath width is the primary microstructural parameter that has influenced the ductility. Furthermore, the detailed fracture surface analysis also revealed only the increase in the microvoid size attributed to the increase in α lath width and no evidence of the porosity was found on the fracture surfaces. This confirms that the failure location of the test sample has very less porosity that did not influence the tensile properties. However, studies conducted on the fatigue properties of as built and HIPped EBM Ti6Al4V showed that the presence of porosity significantly reduced the fatigue performance as built samples compared to HIPped ones as the cracks tend to initiate from the stress concentration cites associated with the porosity [24,25].

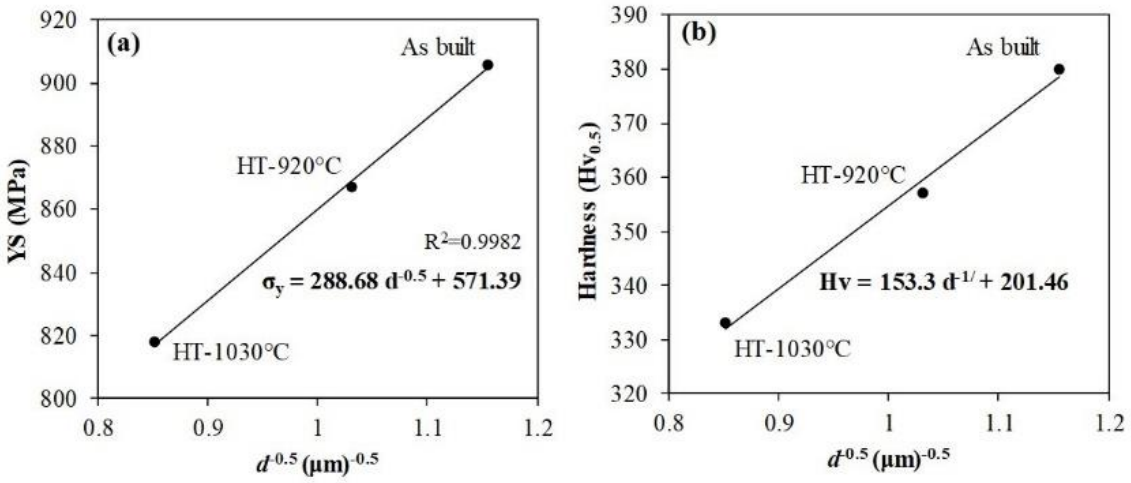

Fig. 8. Hall-Petch relation for as built and heat treated samples showing (a) yield strength as a function of inverse root squared α lath width (b) microhardness as a function of inverse root squared α lath width.

Ti6Al4V alloys exhibits strong grain boundary strengthening or the Hall-Petch effect due to hcp crystal structure [26]. The relationship between yield strength or micro

https://doi.org/10.1080/02670836.2019.1580434

hardness and a specific microstructural scale that is often presented using the Hall-Petch relation was found by [27] and is expressed as follows

$$\sigma_{y=}\,\sigma_0 \;+\; k\,d^{-1/2} \tag{1}$$

$$H_{V=}\,H \;+\; k\,d^{-1/2} \tag{2}$$

where σ_y and H_V is the yield strength and hardness, H_0 and σ_0 is the intrinsic hardness and materials yield strength, d is the average grain size and k, is the Hall–Petch strengthening coefficient.

As mentioned earlier, the mechanical properties of α+β titanium alloys mainly governed by the α phase as its strength is greater than the β phase. Furthermore, the Hall-Petch phenomenon is likely to occur in the α phase rather than in the β phase, according to [26]. Fig. 8 presents the Hall-Petch relationship between yield strength, hardness and α lath width. In general, a good correlation between the change in α lath width and hardness and yield strength is observed. Above results showed a decrease in yield strength and hardness with an increase in α lath width. The good correlation can be evident by the high value of the correlation coefficient, R^2= 0.99. Change in yield strength and hardness with a change in α lath width in EBM Ti6Al4V is also consistent with earlier work reported by [3,11].

Conclusions

The influence of post-process heat treatment on the microstructure and tensile properties of Ti6Al4V produced via electron beam melting was investigated. From the results, the following conclusions are made.

1. As built microstructure consists of homogenous α+β both in the colony and Widmanstätten morphologies within the epitaxially grown prior β grains. The yield and ultimate tensile strengths in as built samples were 5% and 14% higher than that of the wrought material, owing to the fine lamellar α+β microstructure. However, ductility was lower in the additive manufactured.
2. The tensile properties are mainly governed by the α lath width that determines the effective slip length. Heat treatment at 920°C caused 25% increase in ductility and 7% decrease in both the yield strength and tensile strength, whereas heat treatment at 1030°C resulted 125% increase in ductility, with 10% and 17% decrease in yield and tensile strength compared to the as built condition.

https://doi.org/10.1080/02670836.2019.1580434

3. As built sample showed highest density, >99.99%. Post-deposition heat treatment caused porosity re-growth as the gas within the gas pores cannot diffuse out from the material and remains in the samples. Increase in post-deposition temperature has resulted an increase in porosity population; however, it did not affect the ductility.
4. A good Hall-Petch correlation was found between the increase in yield strength and decrease in α lath width.

Disclosure statement

No potential conflict of interest was reported by the authors.

References

[1] Lutjering G, Williams J. Titanium. 2nd ed. 2007.

[2] Antonysamy AA, Meyer J, Prangnell PB. Effect of build geometry on the β-grain structure and texture in additive manufacture of Ti6Al4V by selective electron beam melting. Mater Charact 2013;84:153–68. doi:10.1016/j.matchar.2013.07.012.

[3] Safdar A, Wei LY, Snis A, Lai Z. Evaluation of microstructural development in electron beam melted Ti-6Al-4V. Mater Charact 2012;65:8–15. doi:10.1016/j.matchar.2011.12.008.

[4] Al-Bermani SS, Blackmore ML, Zhang W, Todd I. The origin of microstructural diversity, texture, and mechanical properties in electron beam melted Ti-6Al-4V. Metall Mater Trans A 2010;41:3422–34. doi:10.1007/s11661-010-0397-x.

[5] Hrabe N, Quinn T. Effects of processing on microstructure and mechanical properties of a titanium alloy (Ti-6Al-4V) fabricated using electron beam melting (EBM), part 1: Distance from build plate and part size. Mater Sci Eng A 2013;573:264–70. doi:10.1016/j.msea.2013.02.064.

[6] Hrabe N, Quinn T. Effects of processing on microstructure and mechanical properties of a titanium alloy (Ti-6Al-4V) fabricated using electron beam melting (EBM), Part 2: Energy input, orientation, and location. Mater Sci Eng A 2013;573:271–7. doi:10.1016/j.msea.2013.02.065.

[7] Körner C. Additive manufacturing of metallic components by selective electron beam melting — a review. Int Mater Rev 2016;61:361–77.

doi:10.1080/09506608.2016.1176289.

[8] Murr LE, Esquivel E V., Quinones SA, Gaytan SM, Lopez MI, Martinez EY, et al. Microstructures and mechanical properties of electron beam-rapid manufactured Ti-6Al-4V biomedical prototypes compared to wrought Ti-6Al-4V. Mater Charact 2009;60:96–105. doi:10.1016/j.matchar.2008.07.006.

[9] Xipeng T, Yihong K, Yu Jun T, Guglielmo V, Qing Xiang P, Gang Z, et al. An experimental and simulation study on build thickness dependent microstructure for electron beam melted Ti–6Al–4V. J Alloys Compd 2015;646:303–9. doi:10.1016/J.JALLCOM.2015.05.178.

[10] Lu SL, Tang HP, Ning YP, Liu N, StJohn DH, Qian M. Microstructure and Mechanical Properties of Long Ti-6Al-4V Rods Additively Manufactured by Selective Electron Beam Melting Out of a Deep Powder Bed and the Effect of Subsequent Hot Isostatic Pressing. Metall Mater Trans A 2015;46:3824–34. doi:10.1007/s11661-015-2976-3.

[11] Tan X, Kok Y, Tan YJ, Descoins M, Mangelinck D, Tor SB, et al. Graded microstructure and mechanical properties of additive manufactured Ti-6Al-4V via electron beam melting. Acta Mater 2015;97:1–16. doi:10.1016/j.actamat.2015.06.036.

[12] Sharma H, Parfitt D, Syed AK, Wimpenny D, Muzangaza E, Baxter G, et al. A critical evaluation of the microstructural gradient along the build direction in electron beam melted Ti-6Al-4V alloy. Mater Sci Eng A 2019;744:182–94. doi:10.1016/J.MSEA.2018.12.016.

[13] Facchini L, Magalini E, Robotti P, Molinari A. Microstructure and mechanical properties of Ti-6Al-4V produced by electron beam melting of pre-alloyed powders. Rapid Prototyp J 2009;15:171–8. doi:10.1108/13552540910960262.

[14] Koike M, Martinez K, Guo L, Chahine G, Kovacevic R, Okabe T. Evaluation of titanium alloy fabricated using electron beam melting system for dental applications. J Mater Process Technol 2011;211:1400–8. doi:10.1016/j.jmatprotec.2011.03.013.

[15] Zhai Y, Galarraga H, Lados DA. Microstructure evolution, tensile properties, and fatigue damage mechanisms in Ti-6Al-4V alloys fabricated by two additive

manufacturing techniques. Procedia Eng 2015;114:658–66. doi:10.1016/j.proeng.2015.08.007.

[16] de Formanoir C, Michotte S, Rigo O, Germain L, Godet S. Electron beam melted Ti-6Al-4V: Microstructure, texture and mechanical behavior of the as-built and heat-treated material. Mater Sci Eng A 2016;652:105–19. doi:10.1016/j.msea.2015.11.052.

[17] Mohammadhosseini A, Fraser D, Masood SH, Jahedi M. Microstructure and mechanical properties of Ti–6Al–4V manufactured by electron beam melting process. Mater Res Innov 2013;17:s106–12. doi:10.1179/1432891713Z.000000000302.

[18] Gong H, Gu H, Zeng K, Dilip J., Pal D, Stucker B, et al. Melt pool characterization for selective laser melting of Ti-6Al-4V pre-alloyed powder. 25th Annu. Int. Solid Free. Fabr. Symp., 2014, p. 256–67.

[19] Gong H, Rafi K, Gu H, Starr T, Stucker B. Analysis of defect generation in Ti-6Al-4V parts made using powder bed fusion additive manufacturing processes. Addit Manuf 2014;1:87–98. doi:10.1016/j.addma.2014.08.002.

[20] Tammas-Williams S, Withers PJ, Todd I, Prangnell PB. Porosity regrowth during heat treatment of hot isostatically pressed additively manufactured titanium components. Scr Mater 2016;122:72–6. doi:10.1016/j.scriptamat.2016.05.002.

[21] Lee E, Banerjee R, Kar S, Bhattacharyya D, Fraser HL. Selection of α variants during microstructural evolution in α/β titanium alloys. Philos Mag 2007;87:3615–27. doi:10.1080/14786430701373672.

[22] Dillamore IL, Roberts WT. Preferred orientation in wrought and annealed metals. Metall Rev 1965;10:271–380. doi:10.1179/mtlr.1965.10.1.271.

[23] Ladani L. Erratum to: Local and Global Mechanical Behavior and Microstructure of Ti6Al4V Parts Built Using Electron Beam Melting Technology. Metall Mater Trans A Phys Metall Mater Sci 2016;46:1. doi:10.1007/s11661-016-3402-1.

[24] Hrabe N, Gnaupel-Herold T, Quinn T. Fatigue properties of a titanium alloy (Ti-6Al-4V) fabricated via electron beam melting (EBM): Effects of internal defects and residual stress. Int J Fatigue 2017;94:202–10. doi:10.1016/j.ijfatigue.2016.04.022.

https://doi.org/10.1080/02670836.2019.1580434

[25] Greitemeier D, Palm F, Syassen F, Melz T. Fatigue performance of additive manufactured TiAl6V4 using electron and laser beam melting. Int J Fatigue 2017;94:211–7. doi:10.1016/j.ijfatigue.2016.05.001.

[26] Armstrong R, Codd I, Douthwaite RM, Petch NJ. The plastic deformation of polycrystalline aggregates. Philos Mag A J Theor Exp Appl Phys 1962;7:45–58. doi:10.1080/14786436208201857.

[27] Jung JY, Park JK, Chun CH, Her SM. Hall—Petch relation in two-Phase TiAl alloys. Mater Sci Eng A 1996;220:185–90. doi:10.1016/S0921-5093(96)10446-9.